Z. Phys. B 102, 317–321 (1997)

ZEITSCHRIFT
FÜR PHYSIK B

Vortex core shapes measured by STM

A.P. Volodin[1,*], A.A. Golubov[2,], J. Aarts[1]**

[1] Kamerlingh Onnes Laboratory, University Leiden, P.O. Box 9506, 2300 RA Leiden, The Netherlands
[2] ISI-KFA Jülich, D-52425 Jülich, Germany

Received. 22 July 1996/Revised version: 23 September 1996

Abstract. We have studied vortex core shapes in superconducting $NbSe_2$ by STM, as function of temperature and bias voltage. The experimentally measured tunnel current profiles are compared with the results of calculations using microscopic theory. We find that, at low temperatures ($T/T_c \simeq 0.25$), the apparent vortex core radius strongly depends on the bias voltage, which demonstrates the energy dependence of the scale for spatial variation of the quasiparticle density of states. Good quantitative agreement between measured and calculated profiles is found by using the accepted value for the superconducting coherence length ξ_S, without further adjustable parameters. This shows that the bias dependence is a useful extra tool in the interpretation of local density of states measurements.

PACS: 74.50. + r; 74.70.Jm

1. Introduction

The combination of scanning capability with subnanometer resolution, and spectroscopy with sensitivity in the sub-mV range makes a Scanning Tunneling Microscope (STM) a unique tool to investigate superconducting materials. Especially spatial variations of the superconducting order parameter, which take place on a length scale of the superconducting coherence length, are amenable to such studies. The best known examples of such spatial variations are given by the vortex lattice and the vortex core in a type-II superconductor. With respect to the vortex lattice, first succesfully imaged by Hess et al. [1], a major advantage of the STM is that high magnetic fields can be used, since the vortex cores only start to overlap near the upper critical field B_{c2}; this in contrast to imaging techniques such as decoration or neutron diffraction, which are sensitive to magnetic field gradients, and operate on the (much larger) scale of the superconducting penetration depth λ_s. Vortex core studies are interesting in their own right, since they can provide detailed microscopic information on the quasiparticle Local Density Of States (LDOS). Again in $NbSe_2$, the well-known example is the observation of a zero-bias anomaly in the vortex center [2], interpreted as the signature of Caroli-de Gennes- Matricon bound states [3–5]. More recently, lattice structures and vortex core tunneling spectra were reported for the high-T_c superconductor $YBa_2Cu_3O_7$ [6].

In view of the complex tunneling spectra found in the latter case, and in view of the general questions arising from the fact that the vortex cores in high-T_c materials may have mixed s-d character [7, 8], improving on the understanding of STM data is still of interest. The purpose of the present paper is to study the spatial variation of the tunneling current between vortex centers in the simple s-wave superconductor $NbSe_2$ as function of temperature and bias voltage and to compare the measurements with calculations of the LDOS. Hartmann and Golubov [9] performed a similar study as function of magnetic field, but at constant temperature and bias voltage. Here, we show that at temperatures far below T_c, the decay of the tunnel current with increasing distance to the vortex center strongly depends on the bias voltage, while this dependence is almost absent at higher temperatures. Good quantitative agreement is found with calculated current profiles.

2. Experimental results

STM measurements were performed using a compact low-temperature STM developed in Leiden. For the coarse motion of the tip, a system with differential springs was used, similar to the one described in [10]. The STM was operated in constant-current mode. Typical parameters used to image the vortex lattice were a tunneling voltage

* *Present address*: Laboratory for Solid State Physics and Magnetism, Katholieke Universiteit Leuven, B-3001 Leuven, Belgium
** *Permanent address*: Institute of Solid State Physics, 142432 Chernogolovka, Moscow district, Russia

of ≈ 0.6 mV (sample bias) and a tunneling current less than 10 pA, so that the tunneling resistance was larger than 0.1 GΩ, in order to avoid degradation of the surface by etching with the STM tip [11]. Due to the high sensitivity of our STM, the signal-to-noise ratio decreased to 1 around a quite low tunneling current of about 1 pA at a bias voltage of 0.1 mV. The STM was controlled by commercial electronics and software (RHK Technology). The tips were made by cutting a Pt/Ir (80%/20%) wire. The measurements in magnetic field were carried out by placing a Sm-Co permanent magnet behind the sample. The small size of the crystals ($1 \times 1 \times 0.1$ mm) ensured homogeneous magnetic fields perpendicular to the sample plane. The magnetic field at the sample surface was calibrated at room temperature with a Hall probe. The sample holder contains a heater, while a RuO_2 film resistor in close proximity to the substrate was used as a thermometer. Fresh sample surfaces were produced by cleaving the $NbSe_2$ samples in air before installing them in the STM.

Vortices were visualised in topographic mode (feedback loop enabled) at a voltage within the gap. In this way, an image of the lattice is obtained by mapping the difference in tunnel characteristics inside and outside the vortex core. This is illustrated in Fig. 1, which shows the difference ΔI between an I–V characteristic in a superconducting region (inset of Fig. 1), and the linear behaviour as extrapolated from high voltage, both taken at 4.2 K. Since such linear behaviour is, in first approximation, found inside the vortex core, the difference shows the sensitivity of the mapping procedure as function of the bias voltage. At the maximum difference, which is of the order of a few pA's, vortices (normal regions and higher conductivity) will appear as mounds on the surface with a height of the order of 1 Å [11, 12]. The height variation is then converted back to a tunnel current using the I(z) calibration of the STM. Of course, the height variations caused by changes in the DOS are superimposed on the signal from the surface topography. In the case of $NbSe_2$, the sample usually only reveals atomic corrugation of about 0.1 Å, and vortices are clearly visible in the STM images. Fig. 1 also shows the derivative of the I-V characteristic; the peak in the quasiparticle DOS can be seen at 0.9 mV, which is taken as a measure for the gap Δ, in good agreement with the value reported in [1] at the same temperature of 4.2 K. Note that the peak in ΔI lies at an appreciably lower bias voltage than the peak in dI/dV. Direct imaging therefore allows working at lower bias than imaging of the derivative in ac mode.

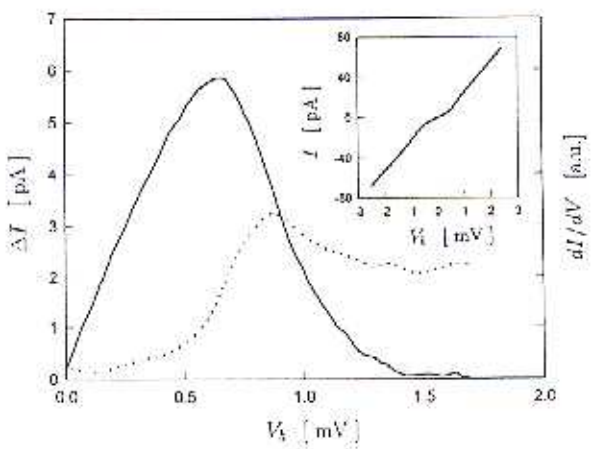

Fig. 1. The full line shows the current difference ΔI as function of bias voltage between the measured superconducting tunnel current and the linear behaviour as extrapolated from high voltages. The insert shows the orginal IV-characteristic. The dotted line shows the derivative of that IV-characteristic

An advantage of the topographic mode (continuous scan as opposed to a step/measure cycle) is that it is fast, and, for vortex lattice imaging, not very critical to the choice of bias value within the superconducting gap. This is also the case for imaging the tunnel current decay away from the vortex center, but some care has to be taken by choosing the scan speed. For a given bias, it is necessary to adjust the bandwidth of the feedback such that the small current difference of about 5 pA still can be detected. The spatial resolution Δs depends on this bandwidth $\Delta\omega$ according to the simple relation $\Delta s = v_s/\Delta\omega$, with v_s the scan speed. To keep the resolution constant, v_s was adjusted in a range 0.3–3 μm/s.

In the experiments, the sample was cooled to a temperature of 1.8 K in a field of 0.3 T; the vortex cores were imaged at constant field with increasing temperature up to 6 K, at a (near-optimum) bias voltage of 0.5 mV. Grey-scale images are shown in Fig. 2. They clearly show that

Fig. 2. Vortex lattice images measured at $V_t = 0.5$ mV, at different temperatures as indicated

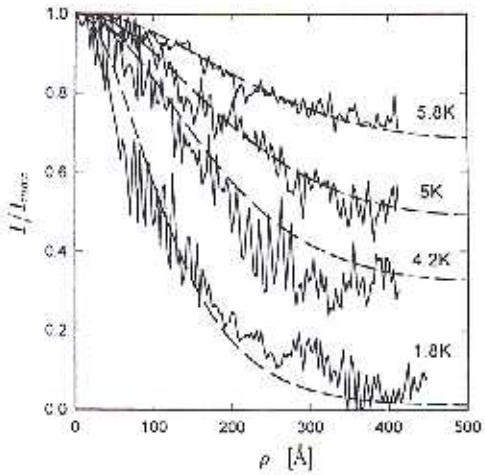

Fig. 3. Decay of the tunneling current as function of distance from the vortex center ρ, measured at $V_b = 0.5$ mV. Drawn lines are measured currents, scaled on the value at $\rho = 0$. Dotted lines are the results of the calculations, using $\xi_s = 5.5$ nm

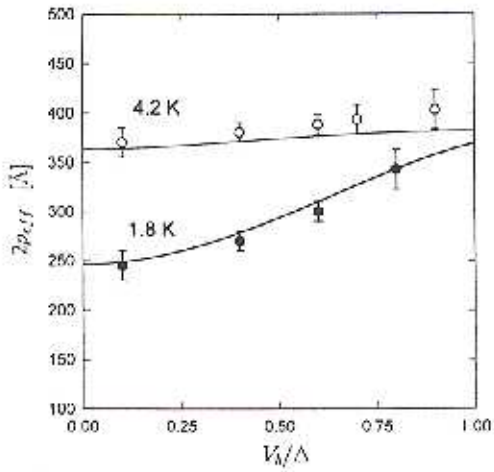

Fig. 4. The effective vortex diameter $2\rho_{eff}$ as defined in the text, as function of bias voltage V_b scaled on the superconducting gap Δ. Open and closed circles show the measurements at 4.2 K and 1.8 K, respectively. The full lines are the results of the calculations, using $\xi_s = 5.5$ nm

the area which can be called the vortex core expands with increasing temperature. The diameter is related to the superconducting coherence length $\xi_s = \sqrt{\hbar v_F l/6\pi T_c}$ (dirty limit), with v_F the Fermi velocity, l the mean free path, and T_c the superconducting transition temperature. More precisely, within the computation of the LDOS using standard microscopic theory, reiterated in Appendix A, the scale for the spatial variation of the LDOS is set by an effective coherence length ξ_{eff}. This length depends on temperature but now also on energy, and grows for $\varepsilon/\Delta \to 1$, with ε the quasiparticle energy and Δ the microscopic order parameter. The energy dependence is the physical origin of the increase of the measured vortex radius with bias. Measurements of temperature and bias dependence will be shown next.

Figure 3 shows measurements of the tunnel current as function of distance from the vortex center in a wide range of temperatures $0.25 \leq T/T_c \leq 0.82$. They were performed at near-optimum bias voltage $V_b \simeq 0.53$ mV, where the current difference between vortex center and superconducting material is about 5 pA (see Fig. 1). The scans represent cross-sections from the vortex center to its periphery, and are scaled on the (maximum) current at the center. Note that the reduced temperature $T/T_c \simeq 0.25$ is still rather high, and the vortex cores were rotationally symmetric with roughly Gaussian shape, rather than showing the sixfold perturbation related to interactions with the crystal lattice [2]. Vortex-core profiles were calculated from (1) (see Appendix A) for various bias and temperatures by numerically solving the Usadel equations (2–5), using a field of 0.3 T. For the coherence length, the critical field slope was determined as function of temperature by resistivity measurements on a sample from the same batch as used in the STM investigation. The measured values of $dB_{c2}/dT \simeq -0.65$ T/K and $T_c = 7.1$ K yield $\xi(0) = 8.5$ nm and $\xi_s = 5.5$ nm; the latter was used in the calculation. The computed curves are shown as dotted lines and show very good agreement with the measurements.

From both measured and calculated curves, we can define an effective radius ρ_{eff} as $I(\rho_{eff}) = 0.36(I_{max} - I_{min})/I_{max}$, or the distance at which the current has decayed to 36% above its minimum value. The values for ρ_{eff} can be used to parameterize the bias dependence of the vortex core shape. In these measurements, we used line scans along nearest-neighbour rows of vortices. Measurements and calculations are shown in Fig. 4, for different bias voltages and two temperatures, 4.2 K and 1.8 K. At high temperature almost no change is found, but at low temperature we find a significant change in effective diameter as function of bias voltage, of the order of 50%. The very satisfactory agreement with the theoretical calculations shows that this effect can be seen as a direct manifestation of the energy dependence of the effective coherence length in a conventional s-wave superconductor. The effect originates from the BCS coherence factors, and should vanish in a pure d-wave case. We believe therefore that the bias voltage dependence may be a useful extra tool when data from High-T_c materials become available, and have to be compared to non-s-wave models.

We would like to acknowledge J.V. Waszczak for providing the crystals. This work is part of the research programs of the 'Stichting voor Fundamenteel Onderzoek der Materie' and of the 'Stichting Technische Wetenschappen', which are financially supported by 'NWO' and the Netherlands Department for Economic Affairs. The work of A. Golubov was also partially supported by NATO Linkage Grant HTECH 930049.

Appendix A: the model calculations

To calculate the decay of the tunnel current or the effective vortex radius, we assume dirty limit conditions, i.e. the mean free path l is shorter than the BCS coherence length $\xi_0 = \hbar v_F/2\pi T_c$. The superconducting coherence length then is $\xi_s = \sqrt{\xi_0 l/3}$. We further assume that the vortices

form a regular lattice. Then, the Wigner-Seitz method can be applied with sufficient accuracy by introducing a circular unit cell with radius $\rho_s = (\Phi_0/\pi H)^{1/2}$ [13]. Under these assumptions the vortex structure within a unit cell can be studied on the basis of the microscopic Usadel equations [14] as was first done by Watts-Tobin et al. [15], who calculated the DOS-averaged order parameter over the unit cell at arbitrary temperatures and magnetic fields. In order to extract the necessary *local* information, this method was developed further in [16] for the calculation of $I-V$ curves of a Josephson junction containing Abrikosov vortices, and in [9] for the study of the field dependence of the STM vortex-core radius. Here we extend these calculations in order to study temperature and bias dependence of a vortex radius and to make a quantitative comparison with experiment.

In the Wigner-Seitz approximation, the STM current at a given bias V_b only depends on the distance ρ from the vortex center and is given by the following expression

$$I(\rho, V_b) = \frac{1}{2eR_0}\int_{-\infty}^{+\infty} d\varepsilon \left[\tanh\left(\frac{\varepsilon + eV_b}{2T}\right) - \tanh\left(\frac{\varepsilon}{2T}\right)\right] N_s(\rho, \varepsilon) \tag{1}$$

where R_0 is the normal state resistance of a contact and $N_s(\rho, \varepsilon)$ is the normalized quasiparticle density of states in a superconductor for an energy ε at a distance ρ from the vortex center. To calculate $N_s(\rho, \varepsilon)$ it is convenient to make the substitution $N_s = Re[\cos\theta(\rho, \varepsilon)]$ where the complex function θ satisfies the Usadel equations

$$\theta''(\rho, \varepsilon) + \frac{1}{\rho}\theta'(\rho, \varepsilon) + \frac{1}{2}Q^2(\rho)\sin 2\theta(\rho, \varepsilon) + i\varepsilon \sin\theta(\rho, \varepsilon) + \Delta(\rho)\cos\theta(\rho, \varepsilon) = 0 \tag{2}$$

where the prime means the derivative with respect to ρ. The gradient-invariant vector potential $Q(\rho)$, in the limit $\kappa \gg 1$, is given by

$$Q = \frac{1}{\rho} - \frac{\rho}{\rho_s^2}. \tag{3}$$

where ρ is normalized to ξ_s and the magnetic field in ρ_s to $\Phi_0/2\pi\xi_s^2$. The boundary conditions for $\Delta(\varepsilon, \rho)$ at the center and the edge of the unit cell are given by:

$$\Delta(0) = \theta(\varepsilon, 0) = 0, \quad \Delta'(\rho_s) = \theta'(\varepsilon, \rho_s) = 0\,. \tag{4}$$

In order to determine $\Delta(\rho)$, these equations are supplemented by the selfconsistency equation

$$\ln\left(\frac{T}{T_c}\right) + 2\pi T \sum_{\omega_n}\left[\frac{\Delta}{\omega_n} - \sin\theta(\rho, \varepsilon = i\omega_n)\right] = 0 \tag{5}$$

where $\omega_n = \pi T(2n+1)$ is the Matsubara frequency. Both Δ and θ are normalized to πT_c.

Analytical solutions of (2–5) can be obtained in the field range near H_{c2}, as discussed in [9, 15, 16]. With these solutions the Maki-de Gennes equation [17] for H_{c2} can be obtained:

$$\ln\left(\frac{T}{T_c}\right) = \psi\left(\frac{1}{2} + \frac{T_c}{T}\frac{\pi\xi_s^2 H_{c2}}{\Phi_0}\right) - \psi\left(\frac{1}{2}\right) \tag{6}$$

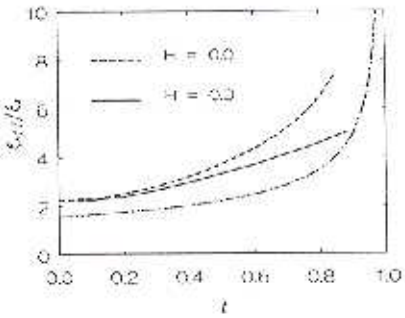

Fig. 5. The temperature dependence of ξ_{eff} as defined in the text, for H = 0 (dashed line) and for H = 0.3 T (drawn line). Also shown is the temperature dependence of the Ginzburg-Landau coherence length $\xi_{GL}(t)$ (dash-dotted line). Note that with the parameters used for $NbSe_2$, a critical field of 0.3 T is reached at $t = 0.93$

where $\psi(z)$ is the digamma function. At zero temperature an important relation between $H_{c2}(0)$ and ξ_s follows from (6)

$$\Phi_0 = 4\pi\gamma^*\xi_s^2 H_{c2}(0)\,, \tag{7}$$

Even without doing the full numerical calculation, it can be seen from (2) that the spatial variation of θ, and consequently of $N(\varepsilon) = \cos\theta$ is given by an energy-dependent length scale ξ_{eff}. At large distances $\xi_s \ll \rho \ll \rho_s$, the gradient and current terms in (2) can be neglected, so that it can be written in the form

$$\xi_{eff}^2\theta'' + \sin(\theta + \alpha) = 0\,, \tag{8}$$

with $\alpha = \tan^{-1}(i\Delta/\varepsilon)$. Simple algebraic analysis shows that $(\xi_{eff})^2 = \xi_s^2/\sqrt{1-(\varepsilon/\Delta)^2}$, which grows when the quasiparticle energies approach Δ. Defined in this way, ξ_{eff} is both field and temperature dependent through Δ. It is instructive to compare the temperature dependences of $\xi_{eff}(t)$ and the Ginzburg-Landau coherence length $\xi_{GL}(t) = \xi_{GL}(0)/\sqrt{1-t}$, which has been done in Fig. 5 for two values of the magnetic field, H = 0 and H = 0.3 T. The increase of ξ_{eff} is clearly more gradual than the square root singularity in ξ_{GL}, which is essentially what is observed in Figs. 2 and 3.

References

1. Hess, H.F., Robinson, R.B., Dynes, R.C., Valles Jr. J.M., Waszczak, J.V.: Phys. Rev. Lett. **62**, 214 (1989)
2. Hess, H.F., Robinson, R.B., Waszczak, J.V.: Phys. Rev. Lett. **64**, 2711 (1990)
3. Shore, J.D., Huang, M., Dorsey, A.T., Sethna, J.P.: Phys. Rev. Lett. **62**, 3089 (1989)
4. Gygi, F., Schluter, M.: Phys. Rev. B **41**, 822 (1990)
5. Klein, U.: Phys. Rev. B **41**, 4819 (1990)
6. Maggio-Aprile, J., Renner, Ch., Erb, A., Walker, E., Fisher, Ø.: Phys. Rev. Lett. **75**, 2754 (1995)
7. Berlinsky, A.J., Fetter, A.L., Franz, M., Kallin, C., Soininen, P.I.: Phys. Rev. Lett. **75**, 200 (1995)
8. Ichioka, M., Enomoto, N., Hayashi, N., Machida, K.: Phys. Rev. B **53**, 2233 (1996)
9. Golubov, A.A., Hartmann, U.: Phys. Rev. Lett. **72**, 3602 (1994)

10. Altfeder, I.B., Volodin, A.P., Khaikin, M.S.: Instrum. Exp. Tech. **32**, N5 (1990) (Plenum Publishing); translated from 'Pribory y Tekhnika Éxperimenta', 5, p188 (september-october 1989)
11. Volodin, A.P., Aarts, J.: Physica C **235-240**, 1909 (1994)
12. Behler, S., Pan, S.H., Jess, P., Baratoff, A., Güntherodt, H.-J., Lévy, F., Wirth, G., Wiesner, J.: Phys. Rev. Lett. **72**, 1750 (1994)
13. Ihle, D.: Phys. Status Solidi (b) **47**, 423 (1971)
14. Usadel, K.: Phys. Rev. Lett. **25**, 560 (1970)
15. Watts-Tobin, R., Kramer, L., Pesch, W.: J. Low Temp. Phys. **17**, 71 (1974)
16. Golubov, A.A., Kupriyanov, M.Yu.: J. Low Temp. Phys. **70**, 83 (1988)
17. Saint-James, D., Sarma, G., Thomas, E.J.: Type II superconductivity, Braunschweig: Pergamon Press 1969